The Astrophysical Journal, 668:708–720, 2007 October 20
© 2007. The American Astronomical Society. All rights reserved. Printed in U.S.A.

THIRTY YEARS OF CONTINUUM AND EMISSION-LINE VARIABILITY IN NGC 5548

S. G. Sergeev,[1,2] V. T. Doroshenko,[2,3] S. A. Dzyuba,[1,4] B. M. Peterson,[5] R. W. Pogge,[5] and V. I. Pronik[1,2]

Received 2006 August 20; accepted 2007 June 1

ABSTRACT

We analyze a total of 827 optical spectra of NGC 5548 obtained over the 30 year period 1972–2001 for the purpose of studying the long-term behavior of the broad Hβ line profile. The variability characteristics, such as mean continuum and emission-line fluxes, rms variability amplitude, autocorrelation functions, and cross-correlation results, are found to be similar for CCD spectra obtained during the period 1989–2001 and for archival pre-CCD spectra from 1972 to 1988. The only significant difference between these two sets of data is that the mean Hβ flux is higher for 1972–1988. While the Hβ profile can vary dramatically on timescales of months to years, the mean profiles for these two periods are similar, but not identical. We searched for correlations among Hβ profile parameters (such as line width, line centroid, blue-to-red ratio of the line wing fluxes) and investigated their relationship to the continuum flux. Only trivial correlations were found, specifically the correlation between continuum and line fluxes and the anticorrelation between line width and line flux, the latter following from the former and from the inverse correlation between line time lag and line width expected for gravitationally dominated motion.

Subject headings: galaxies: active — galaxies: individual (NGC 5548) — galaxies: nuclei — galaxies: Seyfert

1. INTRODUCTION

The central engine in active galactic nuclei (AGNs) produces a time-variable high-energy continuum that ionizes and heats surrounding gas, which produces broad emission lines. Thus the emission-line properties are directly connected to the continuum properties and to the geometry, kinematics, and physical conditions within a region of this gas, referred to as the broad-line region (BLR). Correlations between observed broad-line and continuum properties provide powerful diagnostics of the structure, kinematics, and physical conditions of the BLR. Line emission from photoionized BLR gas responds to the variations of the ionizing continuum and the line response can be used to determine the size and structure of the BLR via reverberation mapping (Blandford & McKee 1982; Peterson 1993). The observed high degree of correlation between emission-line fluxes and the optical continuum fluxes suggests that the fluxes from the optical and ionizing continua must be highly correlated as well. However, the relationships between line fluxes, optical continuum fluxes, and ionizing continuum fluxes are not necessarily linear. For example, an inverse correlation between line equivalent width and continuum flux can be parameterized as a power-law relationship between line and continuum fluxes, $F_{\rm line} \propto F_{\rm cont}^{b}$, where $b < 1$. This is commonly referred to as the "intrinsic Baldwin effect" (e.g., Kinney et al. 1990; Pogge & Peterson 1992; Gilbert & Peterson 2003; Goad et al. 2004).

While the total line fluxes usually follow the continuum fluxes closely, the profile variations are often completely independent of the continuum variations (Wanders & Peterson 1996). Moreover, at least some AGNs show very strong variations in broad-line profiles, such as changes in asymmetry or appearance/disappearance of some profile substructures (e.g., red or blue bumps), although these variations occur over relatively long timescales, typically from months to years (e.g., Wanders & Peterson 1996; Gilbert et al. 1999; Sergeev et al. 2001). Given the much longer timescale for emission-line profile variations compared to continuum variations, it seems likely that the profile substructures are not reverberation effects at all. Several scenarios have been suggested to account for the observed profile variations, including binary black holes (Gaskell 1983, 1996; Peterson 1987), a small number of large clouds or filaments in Keplerian orbits (Anderson 1971), possibly illuminated by beamed emission from the continuum source (Wanders et al. 1995; Goad & Wanders 1996; Wanders & Peterson 1996), outflowing biconical gas streams (Anderson 1971; Veilleux & Zheng 1991; Zheng et al. 1991), inhomogeneities in the disk surface brightness (Zheng et al. 1991; Chakrabarti & Wiita 1994; Gilbert et al. 1999; Sergeev et al. 2000), or multiple physical components in the BLR (Stirpe et al. 1988; Peterson et al. 1990; Sergeev et al. 2001).

Long-term monitoring campaigns enable the study of line-continuum correlations and long-term evolution of the broad-line profiles in order to evaluate changes in the size and physical conditions of the BLR and to distinguish among various BLR models. Some of the most intensive and long-term multiwavelength monitoring programs have been carried out on the Seyfert 1 galaxy NGC 5548, which is now among the best-studied AGNs. In particular, NGC 5548 has been the target of an intensive 13 year monitoring campaign in the optical by the International AGN Watch consortium (see Peterson et al. 2002 and references therein). There have also been concurrent satellite-based observations of NGC 5548 in the ultraviolet (Clavel et al. 1991; Korista et al. 1995), the extreme ultraviolet (Marshall et al. 1997), and X-rays (Markowitz & Edelson 2004). Prior to this, optical observations had been carried out since the 1970s (e.g., Anderson 1971; Chuvaev 1987). From this large database, many valuable results have been obtained on the BLR size, black hole mass, intrinsic Baldwin effect, the relationship between lag and continuum flux, the relationship between optical and UV continuum fluxes, etc. It was also found that the broad-line profiles in NGC 5548 are complex and strongly variable (e.g., Peterson et al. 1987, 1990; Stirpe et al. 1988; Wanders & Peterson 1996). The best-studied broad-line profile is that of Hβ

[1] Crimean Astrophysical Observatory, P/O Nauchny, Crimea 98409, Ukraine; sergeev@crao.crimea.ua, vpronik@crao.crimea.ua.

[2] Isaac Newton Institute of Chile, Crimean Branch.

[3] Crimean Laboratory of the Sternberg Astronomical Institute, P/O Nauchny, Crimea 98409, Ukraine; vdorosh@sai.crimea.ua.

[4] Postgraduate student of the Crimean Astrophysical Observatory; dz-sveta@yandex.ru.

[5] Department of Astronomy, The Ohio State University, 140 West 18th Avenue, Columbus, OH 43210-1173; peterson@astronomy.ohio-state.edu, pogge@astronomy.ohio-state.edu.

TABLE 1
SOURCES OF SPECTROSCOPIC OBSERVATIONS

Data Set Code	Telescope	Detector	Period Covered (JD − 2,440,000)	Number of Spectra
PTG	2.6 m Shajn	Image-tube photography	1420–8449	241
IDS	1.8 m Perkins	Image-tube dissector scanner	5735–7234	28
A	1.8 m Perkins	CCD	7517–10980	259
H	3.0 m Lick Shane	CCD	7777–12,045	54
M	3.5 m and 2.2 m Calar Alto	CCD	7512–9083	36
W1	2.6 m Shajn	CCD	8630–8895	24
W2	2.6 m Shajn	CCD	8983–12,174	185
Total				827

on account of the large amount of data available covering this spectral region.

In the present study, we use original optical spectra of NGC 5548 from early observations carried out in 1972–1990 (Chuvaev 1987) and in 1986–1988 (Peterson et al. 1990), together with more recent spectra obtained by the International AGN Watch consortium in 1989–2001 (Peterson et al. 2002 and references therein). These data sets are intercalibrated to produce homogeneous continuum and Hβ light curves (§ 2). The narrow-line contribution to the broad Hβ is determined and the narrow Hβ and [O III] lines are subtracted from the broad Hβ profile (§ 2.1). Variability characteristics of the Hβ emission line and continuum, as well as cross-correlation results, are compared between pre-CCD spectra from 1972 to 1988 and CCD spectra from 1989 to 2001 (§ 2.2). Changes in the line-continuum correlations are discussed in § 2.3, and line-profile variations, including flux correlations and correlations of the profile parameters, are analyzed in § 2.4. We summarize our results in § 3. In the Appendix, we briefly describe methods for determining the uncertainties for quantities computed in this paper.

2. OBSERVATIONS AND DATA PROCESSING

To study the long-term evolution of the broad Hβ line profile in NGC 5548, we have used archival data obtained in 1972–1990 and CCD spectra obtained during the International AGN Watch program in 1989–2001. A summary of the data sets used in this study is given in Table 1. The archival data consist of photographic spectra acquired with an image tube at the 2.6 m Shajn Telescope of the Crimean Astrophysical Observatory and spectra acquired with the Ohio State Image Dissector Scanner (Byard et al. 1981) at the 1.8 m Perkins Telescope (Peterson et al. 1990). We refer these two data sets to as "PTG" and "IDS," respectively.

The PTG spectra were obtained by K. K. Chuvaev beginning in 1972. These observations were carried out with the same telescope and spectrograph as that of data set "W" from the International AGN Watch papers, but with a slightly narrower slit width of 1″–2″. The typical slit width for these observations was 1.7″.

The IDS spectra are almost identical to those of data set "A" from the International AGN Watch papers, although they are somewhat noisier. The differences between these are the detectors and aperture geometry, but the aperture areas are the same for both sets of observations.

From the CCD spectra, we have only used the larger higher quality data sets, i.e., "A," "H," "M," and "W" (see Peterson et al. 2002 and references therein). Calibration in flux, intercalibration between different data sets, and measurements of the Hβ line and continuum fluxes have been performed in the fashion described by Peterson et al. (1991). Intercalibration is necessary to account for systematic differences in the broad-line and continuum fluxes between different data sets after spectral scaling using narrow-line fluxes. The entrance aperture admits flux from the pointlike nonstellar continuum and BLR, as well as from the spatially extended host galaxy and narrow-line region. Therefore, the ratio of fluxes of these sources should be aperture dependent, as well as seeing dependent. Each individual data set has been adjusted to the standard data set "A" to account for differences in the entrance apertures. The data set "W" actually consists of two subsets with entrance slit widths of 2.3″ and 3″, that were, of course, adjusted separately. In Table 1, we designate these subsets as "W1" and "W2," respectively. Fortunately, the IDS data do not require any adjustment as mentioned above. The PTG data set has many quasi-simultaneous observations with both the IDS and "A" data sets, and, therefore, can be easily adjusted to the data set "A." Note that the PTG spectra from 1989–1990 were used only for intercalibration purposes: we did not use them for further analysis, because much higher quality CCD spectra are available for these years. For the purpose of intercalibration, we adopt a time interval of four days as "quasi-simultaneous." With this criterion, the PTG data set has 15 data points that can be compared with the IDS data set and 9 data points that can be compared with data set "A." From these quasi-simultaneous pairs of observations, we determined the intercalibration constants $\varphi = 0.832$ and $G = -1.19 \times 10^{-15}$ ergs cm^{-2} s^{-1} Å^{-1} (as defined by Peterson et al. 1991). By comparison of the quasi-simultaneous points, we then estimate the mean fractional uncertainties in the measurements for PTG data set to be 8.4% for the Hβ line fluxes and 9.2% for the continuum fluxes. These uncertainties are in very good agreement with the uncertainties derived from the point-to-point scatter (again, assuming a four-day interval for quasi-simultaneous pairs of data points) of 7.8% and 9.5%, respectively.

2.1. *Subtraction of the Narrow Components*

To accurately subtract the narrow components from the broad Hβ line, we have used low-state spectra of NGC 5548 to isolate the narrow-line components. Spectral decomposition has been applied separately to each of the data sets "A," "H," "M," and "W." The far-red wing of the broad Hβ line is blended with the [O III] λ4959 line, and the far-red wing of the [O III] λ4959 is slightly blended with the far-blue wing of the [O III] λ5007 line. We therefore first use the [O III] λ5007 line to represent the blue wing of the [O III] λ4959 line by shifting it to 4959 Å and reducing the flux density across the line by a factor of 2.93. This allows us to free the blue wing of [O III] λ5007 of contamination by the red wing of [O III] λ4959. We then use the corrected [O III] λ5007 line to subtract the [O III] λ4959 line from the spectrum. Following this, we remove the narrow Hβ component by using a deblending algorithm with the [O III] λ5007 line profile as a template for the narrow Hβ line. We fit the template position, width,

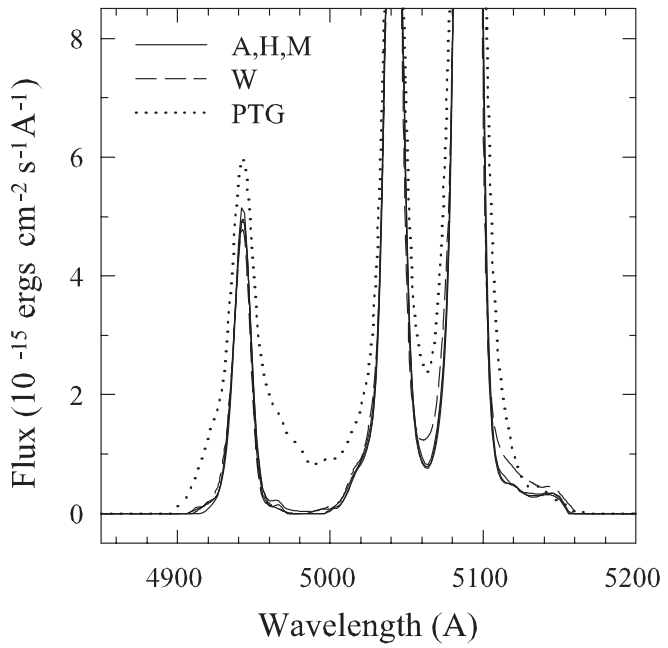


FIG. 1.—Narrow-line profiles subtracted from the spectra of the data set "W" (*dashed line*), data sets "A," "H," and "M" (*solid lines*), and PTG version 2 (*dotted line*). The narrow lines for the IDS data set were assumed to be the same as that of set "A," and narrow lines for the PTG version 1 were assumed to be the same for set "W."

and intensity to try to achieve the smoothest residuals (i.e., the broad-line Hβ profile) when the template is subtracted from the observed Hβ profile. Our models of the narrow lines are shown in Figure 1. We have assumed that the narrow lines for the PTG data set are same as for data set "W" because both data sets were obtained with the same telescope and spectrograph.

The spectra were optimally aligned in wavelength and in spectral resolution for better subtraction of the derived narrow lines. Wavelength shifts and differences in resolution were obtained in the same way as in previous papers on NGC 5548 (e.g., Peterson et al. 2002), based on the scaling algorithm of van Groningen & Wanders (1992). After continuum subtraction and subtraction of the narrow lines, we adjusted each set of spectra by multiplying by the intercalibration constant φ (Peterson et al. 1991). We then compared the broad Hβ line profiles between various data sets to check for consistency. To compare between profiles for two data sets, we have selected quasi-simultaneous pairs of profiles and formed an average for each set. We compare these average profiles in Figure 2. The top panel shows that there is excellent agreement among the CCD data sets "A," "H," "M," and "W." However, there is a noticeable difference between the PTG data set and other data sources, as seen in the two leftmost panels in the bottom row of Figure 2, in the sense that the broad Hβ profiles from the PTG data set have a lower blue-to-red flux ratio in the wings compared to the CCD/IDS data. Some experimentation revealed that this difference can be sharply reduced by assuming that the PTG spectra have an additional quasi-constant contribution to the broad Hβ line. This contribution has been fit in order to achieve consistency between PTG and IDS/CCD. This additional contribution was subtracted from the PTG spectra, and then the PTG data set was recalibrated. The new intercalibration constants were found to be $\varphi = 0.934$ and $G = -8 \times 10^{-17}$ ergs cm^{-2} s^{-1} Å^{-1}. The flux in this additional constant contribution to the broad Hβ line was found to be 9.82×10^{-14} ergs cm^{-2} s^{-1}, and it can be treated as an additive term for the Hβ line. The two rightmost panels in the bottom row of Figure 2 show the comparison between the broad Hβ profiles for this alternative version of the PTG data set, which is in much better agreement with the other data sets.

Thus we have two calibration versions for the PTG data set. The first version is based on the assumption that the narrow-line contribution to the broad Hβ profile is exactly the same as for

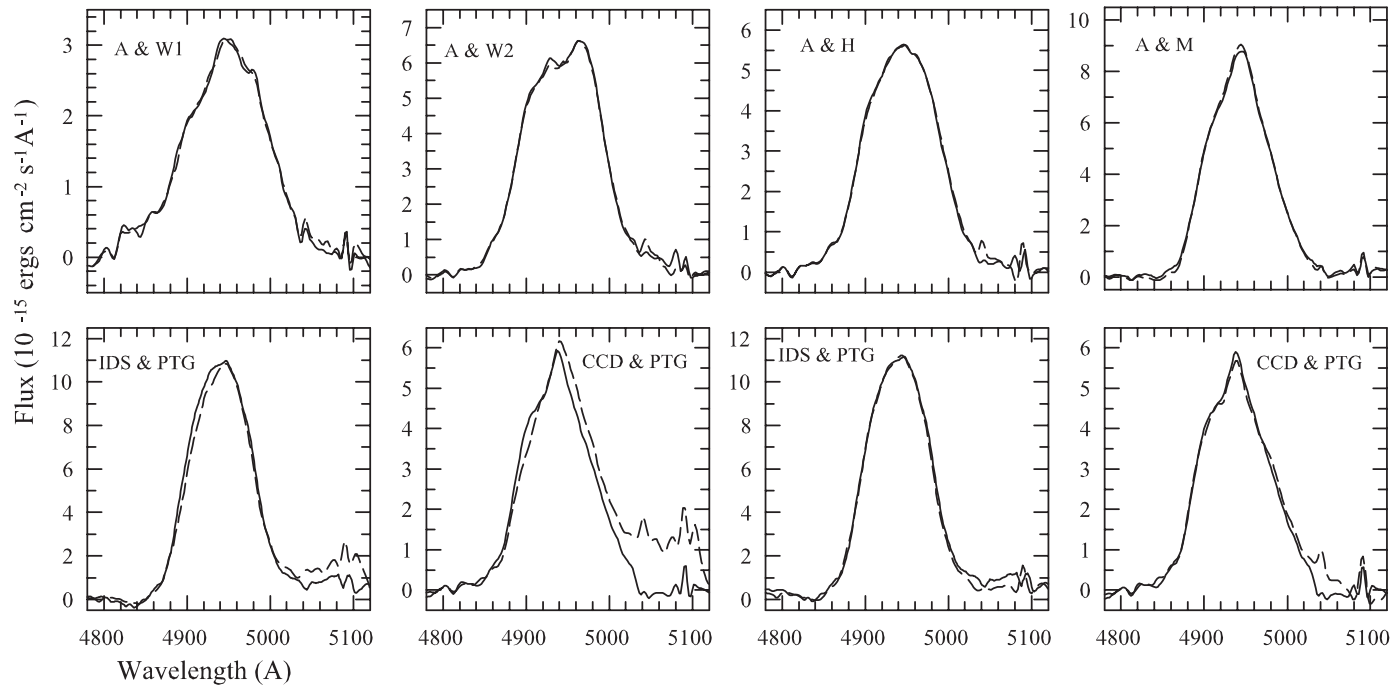


FIG. 2.—Comparison of the Hβ broad component for different data sets after continuum subtraction, narrow-line subtraction, and correction for the intercalibration constant φ. In each panel, we indicate the pair of data sets that are being compared. The solid and dashed lines show the Hβ profile for the first and second data sets, respectively. Only the quasi-simultaneous observations have been used for comparison. The data set designated as "CCD" means all the CCD data, i.e., data sets "A," "H," "M," and "W." The two leftmost panels at the bottom represent versions 1 (*left*) and 2 (*right*) of the PTG data set, as described in the text.

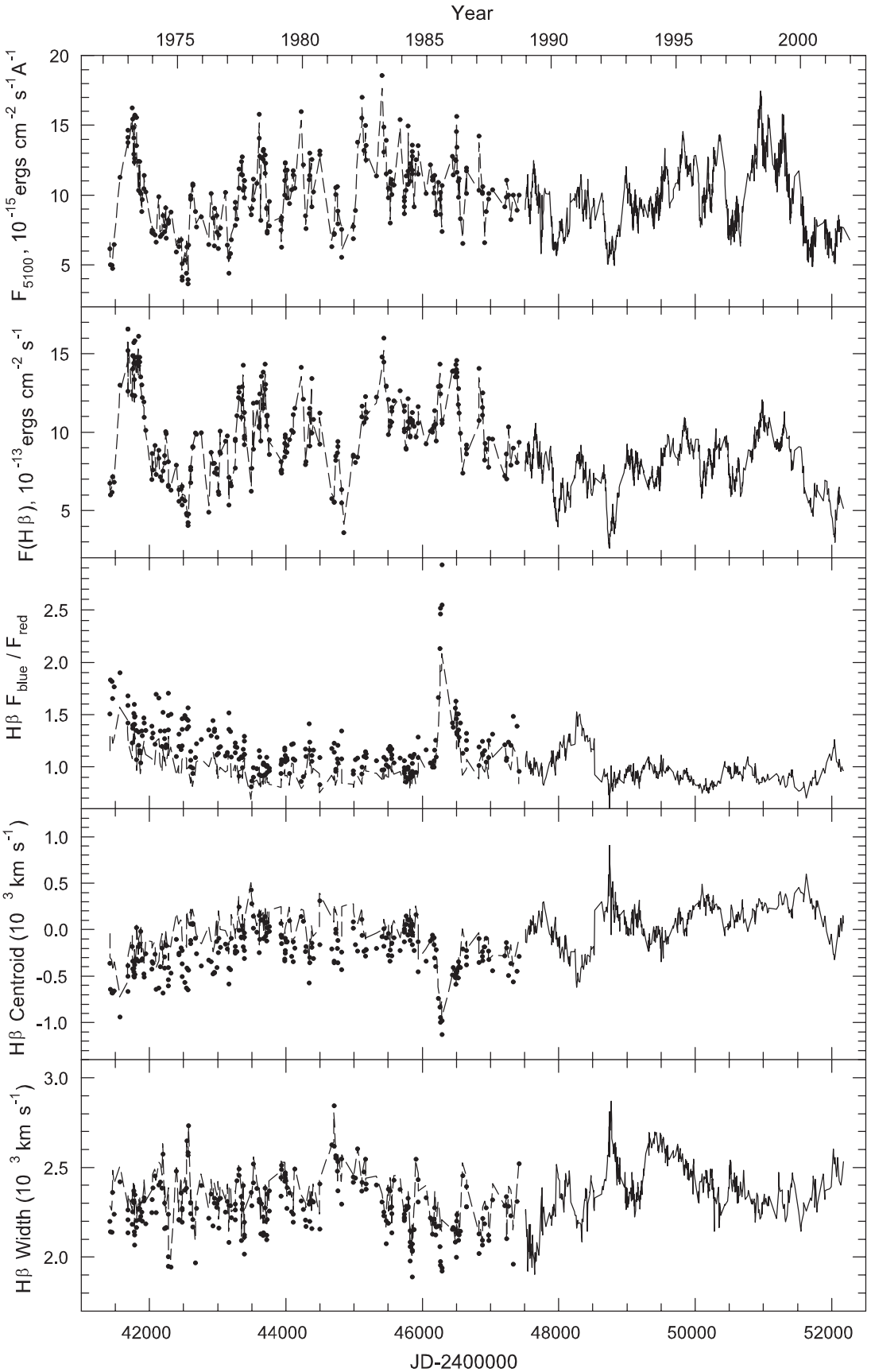


FIG. 3.—Variability of the optical continuum and the Hβ emission line over a 30 year time span. Shown from top to bottom are (1) the continuum light curve at 5100 Å, (2) the Hβ light curve, (3) the blue-to-red ratio of fluxes of the Hβ wings, (4) the Hβ line centroid, and (5) the Hβ width (defined as the profile dispersion $\sigma_{\rm line}$ (see Peterson et al. 2004). The CCD data for 1989–2001 are shown as solid lines, while pre-CCD for 1972–1988 are shown by dashed lines (PTG version 1) and by filled circles (PTG version 2). The Hβ line fluxes and continuum fluxes for the CCD data in the two top panels are from Peterson et al. (2002) and references therein.

TABLE 2
SUMMARY FOR VARIABILITY OF CONTINUUM AND TOTAL Hβ FLUXES

	Continuum Flux			Hβ Flux				
Years	Mean	rms (%)	ACF	Mean	rms (%)	τ_{peak}	τ_{cent}	r_{max}
(1)	(2)	(3)	(4)	(5)	(6)	(7)	(8)	(9)
1972–1988	10.19 ± 0.52	22.8 ± 2.8	164^{+96}_{-36}	10.00 ± 0.52	23.2 ± 3.2	$13.0^{+7.0}_{-4.9}$	$18.3^{+5.8}_{-5.0}$	$0.908^{+0.030}_{-0.036}$
1972–1988	10.17 ± 0.58	25.5 ± 3.1	164^{+96}_{-36}	10.12 ± 0.58	25.4 ± 3.5	$13.0^{+8.8}_{-5.8}$	$18.4^{+6.1}_{-5.0}$	$0.908^{+0.030}_{-0.036}$
1989–2001	9.72 ± 0.72	24.6 ± 4.0	322^{+154}_{-108}	7.82 ± 0.50	21.6 ± 3.4	$17.5^{+1.1}_{-1.1}$	$25.3^{+1.4}_{-1.5}$	$0.941^{+0.024}_{-0.030}$

NOTES.—The first and second rows represent the two different calibrations of the 1972–1988 data, versions 1 and 2, respectively. Units for mean fluxes are 10^{-15} ergs cm^{-2} s^{-1} Å^{-1} for the continuum and 10^{-13} ergs cm^{-2} s^{-1} for the Hβ line.

data set "W," while the second version is based on the assumption that there is an additional constant contribution of an unknown nature. We suspect that it is an instrumental effect, noting in particular the notorious difficulty of obtaining accurate spectrophotometry with photographic detectors. Scattered light might also play a role. Since we cannot confidently reject our original calibration, we will carry through the rest of our analysis using both the original and modified calibration, referring to them as versions 1 and 2, respectively. Fortunately, none of our conclusions depend on which version is used.

We find that the total flux of the narrow Hβ line is 7.70×10^{-14} ergs cm^{-2} s^{-1} and the Hβ/[O III] λ5007 narrow-line flux ratio is 0.138. This is higher than some earlier determinations (e.g., Peterson 1987; Wamsteker et al. 1990), but slightly lower than the value of 0.151 determined by Wanders & Peterson (1996), although the latter value was rejected as too high by Peterson et al. (2004). However, we have found that there is a small contribution to the integration zone of the broad Hβ line (λλ4795–5018) from the far blue wing of [O III] λ4959 and, possibly, from a weak narrow feature at an observed-frame wavelength ∼5017 Å. The total narrow-line contribution to the broad Hβ line is found to be 8.27×10^{-14} ergs cm^{-2} s^{-1}.

2.2. *Variability Patterns of the Continuum and Emission-Line Fluxes*

Our final continuum and Hβ emission-line light curves are shown in the two top panels of Figure 3. In this figure, the narrow-line contribution has not been subtracted from the total Hβ flux. The solid lines show published light curves for the period 1989–2001 from the AGN Watch papers. The dashed lines and filled circles represent versions 1 and 2, respectively, of the PTG[6] data set from 1972 to 1988.

Variability characteristics for the continuum and Hβ fluxes are summarized in Table 2 separately for the two periods of observations, 1972–1988 (pre-CCD) and 1989–2001 (CCD). Column (1) lists the interval over which the data were obtained, and columns (2) and (3) are the mean and rms continuum fluxes. Column (4) is the full width of the autocorrelation function (ACF) at half maximum, i.e., $r = 0.5$. Columns (5) and (6) are the mean and rms Hβ fluxes of the Hβ line, column (7) gives location of the peak value τ_{peak} of the continuum/Hβ cross-correlation function (CCF), and column (8) gives τ_{cent}, the centroid of the peak in the cross-correlation function. The peak value of the CCF r_{max} is given in column (9). The CCF is computed using the interpolation cross-correlation method (Gaskell & Sparke 1986; White & Peterson 1994). Computation of the centroid τ_{cent} is based on points around τ_{peak} with values $r \geq 0.8 r_{max}$. Uncertainties in the values of τ_{cent} and τ_{peak} are computed using the model-independent Monte Carlo flux randomization/random subset selection (FR/RSS) technique of Peterson et al. (1998). Other uncertainties have been computed as described in the Appendix.

In Figure 4, we show the continuum ACF and the continuum/Hβ CCF. Given the large uncertainties in the continuum and Hβ fluxes, especially in the pre-CCD data, we consider here how these

[6] From this point onward, the IDS data set is included with the PTG data set.

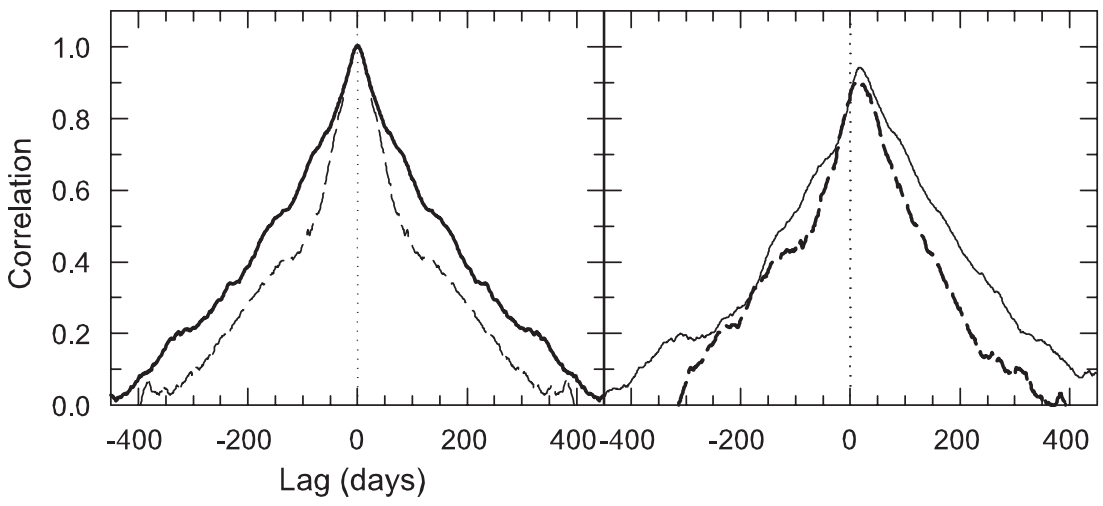


FIG. 4.—*Left panel*: Continuum autocorrelation functions. *Right panel*: Cross-correlation functions of the Hβ line with the continuum. Dashed and solid lines denote the two periods of observations, 1972–1988 and 1989–2001, respectively. All the functions are corrected for observational uncertainties, as described in the text.

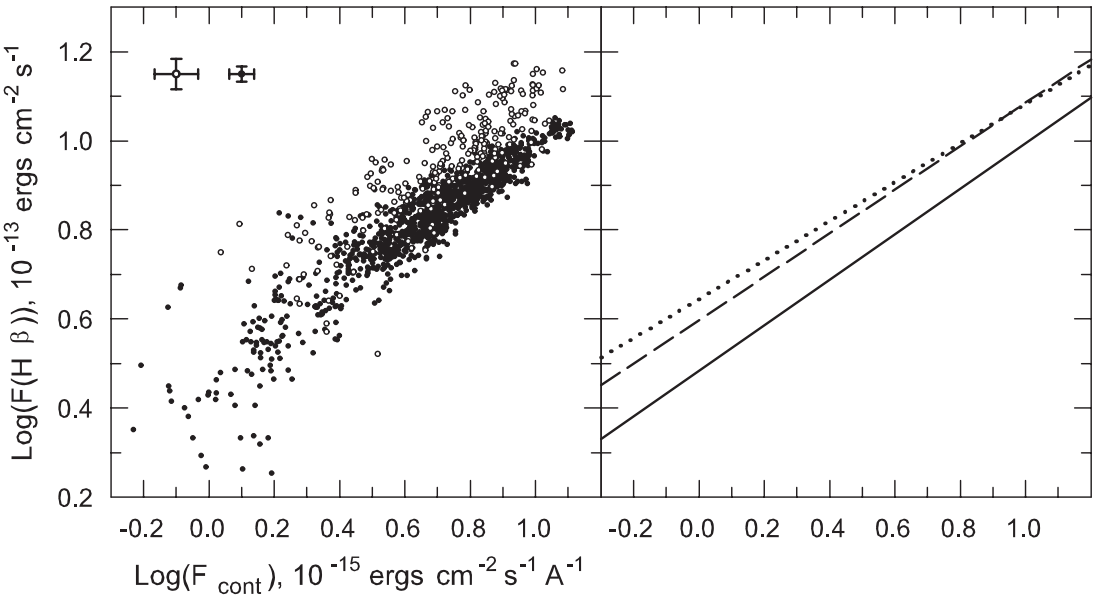


FIG. 5.—Hβ emission-line flux vs. the optical continuum flux. Constant contributions (narrow lines and host galaxy) have been subtracted, and the lag between Hβ fluxes and continuum fluxes has been taken into account. Filled circles are data for 1989–2001 and open circles are data for 1972–1988, version 1. The left panel shows ordinary $y|x$ unweighted regression lines for 1989–2001 (*solid line*) and for 1972–1988 (dashed and dotted lines represent versions 1 and 2, respectively). The two crosses in the left corner illustrate typical uncertainties.

might affect the ACF and CCF. Let us assume that $D_{\rm err}$ is the variance (dispersion) of the observational errors in the light curve, $D_{\rm var}$ is the intrinsic variance of the random process (i.e., intrinsic flux variability), $D_{\rm obs}$ is the observed variance, and $\mathrm{ACF}_{\rm var}(\tau)$ and $\mathrm{ACF}_{\rm obs}(\tau)$ are intrinsic and observed ACFs, respectively. For simplicity, we assume that all the data points have the same variance, so that $D_{\rm obs} = D_{\rm var} + D_{\rm err}$. It does not matter whether the uncertainties are relative or absolute. From the definition of the ACF, we can write $\mathrm{ACF}_{\rm var}(\tau) = \mathrm{ACF}_{\rm obs}(\tau)k$ and $\mathrm{ACF}_{\rm var}(0) = 1$, where $k = D_{\rm obs}/D_{\rm var}$. Here we assume that the width of the ACF due to the observational uncertainties is zero, i.e., a delta function at $\tau = 0$. In reality, this function must be nonzero for $\tau \neq 0$ because observational uncertainties are correlated via the interpolation technique of the computation of the ACF, which, in turn, is dependent on the data sampling: this is the sampling window ACF (cf. Gaskell & Peterson 1987), $\mathrm{ACF}_{\rm samp}(\tau)$. We can then write $\mathrm{ACF}_{\rm var}(\tau) = \mathrm{ACF}_{\rm obs}(\tau)k - \mathrm{ACF}_{\rm samp}(\tau)(k-1)$. In the case of the CCF, if uncertainties in the two time series are assumed to be uncorrelated (although they can be slightly correlated via scaling factors for flux calibration), we have $\mathrm{CCF}_{\rm var}(\tau) = \mathrm{CCF}_{\rm obs}(\tau)k$, where $k = [(DX_{\rm obs}/DX_{\rm var})(DY_{\rm obs}/DY_{\rm var})]^{1/2}$ and DX, DY are variances of these two series.

The continuum ACF and continuum Hβ CCF, corrected for flux uncertainties as described above, are also shown in Figure 4. The values of ACF width, variability amplitudes, and $r_{\rm max}$ in Table 2 are those corrected for observational uncertainties. The effect of these corrections is very small for the CCD data from 1989 to 2001, but much greater for the pre-CCD data because of greater uncertainties in the fluxes. For example, the uncorrected ACF width is 129 days in 1972–1988 and 307 days in 1989–2001, and the uncorrected values of $r_{\rm max}$ are 0.801 and 0.917, respectively.

2.3. *Line-Continuum Relationship*

In this section, we consider the relationship between the Hβ line and continuum fluxes, correlations between various parameters that describe the Hβ line profile, and the correlation between these parameters and continuum flux. Since the Hβ line responds to the continuum variations with some lag, we take this lag into account assuming that the lag is a function of the continuum flux. Each data point of the continuum light curve has been shifted in time according to its flux. The lag-flux dependence for the Hβ line in NGC 5548 was taken from Peterson et al. (2002).

Our pre-CCD data also show correlation between lag and flux at 94% confidence, and this correlation is in accordance, within uncertainties, with the correlation from Peterson et al. (2002). Unfortunately, the uncertainties in the lag measurements are very large ($\sim$25 days for each of the two-year periods). We assumed that the dependence from Peterson et al. (2002) is also valid for the period of our pre-CCD data.

TABLE 3
CONTINUUM-Hβ REGRESSION LINE

	ORDINARY $y|x$		REDUCED MAJOR AXIS		BCES ORTHOGONAL	
YEARS	b	a	b	a	b	a
1972–1988.....	0.488 ± 0.048	3.96 ± 0.33	0.593 ± 0.027	3.33 ± 0.17	0.573 ± 0.031	3.44 ± 0.19
1972–1988.....	0.438 ± 0.045	4.41 ± 0.36	0.541 ± 0.030	3.74 ± 0.21	0.510 ± 0.034	3.94 ± 0.24
1989–2001.....	0.511 ± 0.029	3.05 ± 0.14	0.551 ± 0.010	2.86 ± 0.05	0.548 ± 0.011	2.88 ± 0.05

NOTE.—The first and second rows represent the two different calibrations of the 1972–1988 data, versions 1 and 2, respectively.

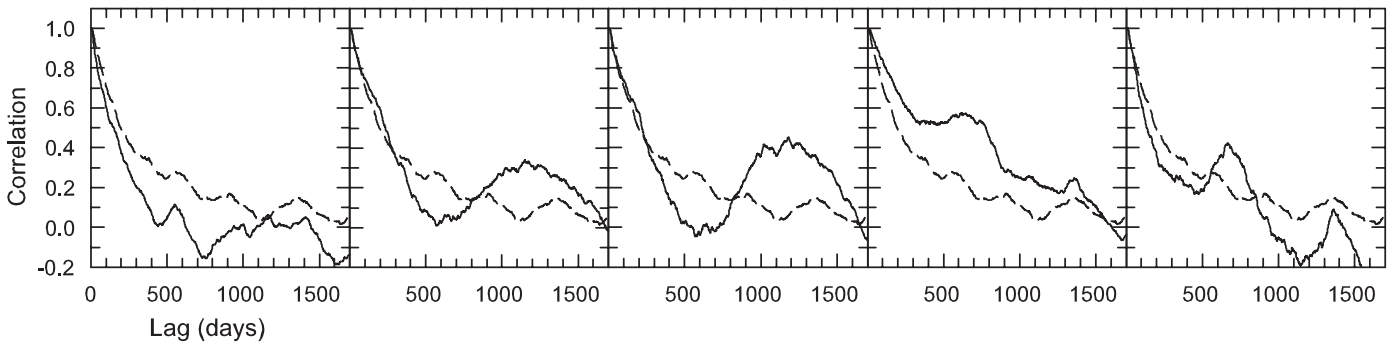


FIG. 6.—Autocorrelation functions for the entire data set. The dashed line in each panel is the autocorrelation function for the Hβ line flux. Solid lines are autocorrelation functions for (*left to right*) the continuum flux, blue-to-red ratio of the Hβ wing fluxes, Hβ centroid, and Hβ width (FWHM and $\sigma_{\rm line}$).

In Figure 5, the Hβ flux is shown as a function of the continuum flux, after an adjustment for the time lag. We have subtracted constant contributions (narrow lines and host galaxy). The host-galaxy flux at 5100 Å was taken to be $F_{\rm galaxy}(5100\ \text{Å}) = 4.47 \times 10^{-15}$ ergs cm^{-2} s^{-1} Å^{-1} (Bentz et al. 2006), while the narrow-line contribution is taken to be 8.27×10^{-14} ergs cm^{-2} s^{-1} (see § 2.1). The right panel of Figure 5 shows ordinary $y|x$ unweighted regression lines computed separately for the two periods of observations, 1972–1988 and 1989–2001. The regression parameters are given in Table 3. Here b is a regression coefficient, i.e., a power-law index for the Hβ-continuum relationship, and $\log a$ is a regression constant, and thus $\log F(\text{H}\beta_{\rm broad}) = \log a + b \log [F_{\rm obs}(5100\ \text{Å}) - F_{\rm galaxy}(5100\ \text{Å})]$.

A similar fit to the same data for 1989–2001 has been performed by Gilbert & Peterson (2003). They found that $b = 0.648 \pm 0.022$ and $a = 2.18 \pm 0.09$. The differences between these results arises from different assumptions for narrow-line and host-galaxy contributions to the Hβ and continuum fluxes, respectively. We believe that the larger uncertainties we quote here, computed as described in the Appendix, are more accurate.

It is well known that the slope b for the ordinary $y|x$ regression is biased toward lower values if there is measurement error in the independent variable. We therefore applied alternate techniques: major axis regression and BCES (bivariate correlated errors and intrinsic scatter, see Akritas & Bershady 1996) orthogonal regression. The regression coefficients for both alternate methods (see Table 3) seem to be more realistic, while our method for uncertainty estimates provides more realistic uncertainties for the ordinary regression coefficients.

Since the power index b is significantly less than unity, the equivalent width of the Hβ line must decrease with increasing continuum brightness, i.e., EW $\propto F(\lambda 5100)^{b-1}$. This intrinsic Baldwin effect is discussed in the context of NGC 5548 by Gilbert & Peterson (2003), Goad et al. (2004), and Cackett & Horne (2006).

We have also attempted to determine through some simple simulations how b is affected by geometrical dilution of the variability signal. We explore this by considering different emission-line transfer functions. We restricted this analysis to the 1989–2001 data, and for simplicity, we considered only transfer functions that do not depend on the continuum flux. We experimented with several kinds of transfer functions for which the CCF has a peak at $\tau = 18$ days. For a delta function $\delta(\tau - 18$ days), we obtain a precisely linear relationship, i.e., $b = 1$. For a top-flat transfer function (constant from 0 to 36 days and zero otherwise, which is the transfer function for a thin spherical shell), we find $b = 0.940$. For the observed Hβ transfer function recovered by Peterson et al. (1994), we find $b = 0.824$. We thus conclude that while the real value of b can be greater than the observed value, the magnitude of the effect is not clear. The effect of the transfer function on the index b was also considered by Gilbert & Peterson (2003), who tested several geometries of the BLR and concluded that the difference in b must be about 0.05 or even less. From the same data for 1989–2001, Cackett & Horne (2006) have recovered a transfer function $\psi(\tau, F_c)$ that is allowed to change with the continuum flux F_c. They find the power index b to be in the range 0.57–0.66 for various models that include particular kinds of the parameterized functions $\psi(\tau, F_c)$ and nonparameterized deconvolutions of $\psi(\tau, F_c)$. However, they used a smaller correction for the host-galaxy contribution, from Romanishin et al. (1995). Their computations also show that the dependence of the Hβ time delay on the continuum flux can be flatter than previously determined by Peterson et al. (2002).

Figure 5 shows a plot of the Hβ flux versus the continuum flux, again adjusted for the lag between them. Inspection of this diagram reveals that relationship between these quantities seems be different in the 1972–1988 data than in the 1989–2001 data. Based on what we believe are realistic uncertainties, the values of the parameter a differ by 2.6 σ or 99.1% confidence (see Table 3), while differences in the power-law index b are less significant. The difference in the Hβ-continuum relationship is also clearly seen from Table 2, as the mean continuum flux changes little between 1972–1988 and 1989–2001, while the mean Hβ flux changes significantly. Gilbert & Peterson (2003) also suggest "possibly that the relationship varies somewhat with time." Goad et al. (2004) measured the power-law index b separately for each of the 13 years of the 1989–2001 monitoring campaign and concluded that b displays significant variation on timescales of around a year. They also concluded that, on average, the power-law index decreases as the continuum flux increases. This is consistent with photoionization model predictions for the BLR in NGC 5548 (Korista & Goad 2004).

A possible explanation for the changes in the parameter a between both periods is either changes in the covering factor of the BLR, changes in the physical properties of the BLR clouds (such

TABLE 4
PARAMETERS OF THE MEAN Hβ PROFILE IN 1972–1988 AND IN 1989–2001

Years	b/r	Centroid (km s^{-1})	FWHM (km s^{-1})	$\sigma_{\rm line}$ (km s^{-1})
1972–1988.....	1.03	−80	5910	2330
1972–1988.....	1.21	−240	6020	2270
1989–2001.....	0.96	+80	6490	2400

NOTE.—The first and second rows represent the two different calibrations of the 1972–1988 data, versions 1 and 2, respectively.

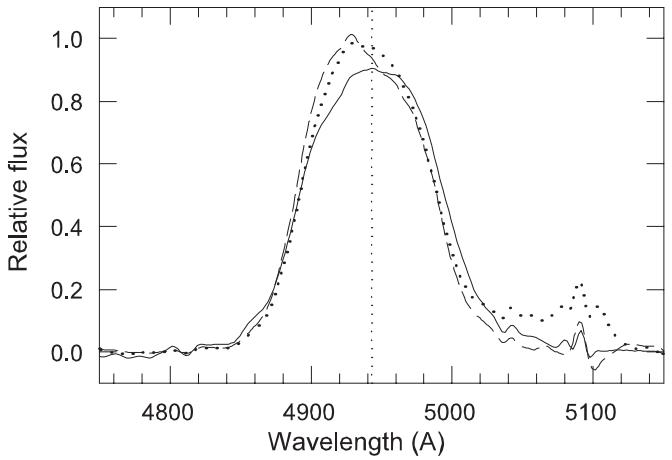


FIG. 7.—Mean broad Hβ profiles in 1989–2001 (*solid line*) and in 1972–1988 (dotted and dashed lines for versions 1 and 2, respectively).

as internal densities or internal velocity dispersions), or changes in the relationship between optical and ionizing continuum fluxes: $F_{\rm opt} = aF_{\rm ion}^{b}$, specifically changes in the factor a. Taking into account that the Hβ profile changed a little between both periods, it seems to be likely that the average volume-filling factors, BLR kinematics, and cloud physical properties remain approximately the same over a long time, so the last explanation seems to be more plausible.

2.4. *Evolution of the Line Profile*

Inspection of individual broad Hβ profiles over a 30 year period reveals great diversity. On timescales of years, or less in some cases, the broad Hβ profile can undergo dramatic changes: it can be a typical single-peaked profile centered near the systemic redshift of the galaxy, it can show strong blue or red peaks, or it can change to a double-peaked profile.[7] These profile transformations seem mysterious and difficult to interpret. It seems that the profile evolution is completely random, irregular, and unpredictable. As will be shown below, profile changes, except for the total fluxes, seem to be completely independent of the nuclear brightness, and various profile parameters are poorly correlated with one another.

We have measured total flux, centroid, widths, equivalent width (EW), and blue-to-red ratio of the wing fluxes (b/r) of Hβ from all of the spectra in this study. All these parameters have been computed by integrating over the wavelength range that corresponds to line-of-sight velocities from -6000 km s^{-1} to $+6000$ km s^{-1}. The narrow Hβ and [O III] lines have been subtracted as described earlier. The continuum light curve has been shifted in time to account for the Hβ lag as described above. When computing the Hβ equivalent widths, we have subtracted the host-galaxy contribution from the continuum fluxes. The profile width is characterized in two ways: by full width at half maximum (FWHM) and by the line-profile dispersion or second moment of the profile ($\sigma_{\rm line}$). Since $\sigma_{\rm line}$ is very sensitive to the far wings of the line profile, the profile wings were smoothed prior to measurement.

In Figure 3, we show the evolution of the Hβ profile width, centroid, and b/r over 30 years. It is seen that the Hβ profile parameters show unrelated, apparently random changes on various timescales. Probably the most dramatic change that occurred in the broad Hβ profile on a short timescale was during the period from JD 2446262 to JD 2446289, when the profile developed the strongest blue asymmetry ever observed. This asymmetry was so strong that the profile centroid was shifted to about -1000 km s^{-1}. Of course, the possibility that some kind of systematic error might have persisted through the five PTG spectra during this period (there are no IDS spectra observed for this period) cannot be excluded completely. On the other hand, the IDS spectra show similar asymmetries occurred during the period JD 2446441 to JD 2446493, as was reported earlier by Peterson et al. (1987).

In Figure 6, we show autocorrelation functions for the variations of the Hβ profile parameters for the entire data set with the PTG version 1 (version 2 gives similar ACFs). The ACFs were corrected for observational uncertainties that were determined from the point-to-point scattering. It is seen that the width of the central peak of ACFs is approximately the same for the Hβ profile variations and Hβ flux variations, so the profile variations occur on timescales comparable to the flux variations. However, the far wings of ACFs for the profile variations show secondary peaks at $\approx$1200 days (centroid and b/r) and at $\approx$650 days (FWHM and $\sigma_{\rm line}$). Perhaps it can be interpreted as a long-term quasi-periodical component of the profile variations.

While individual Hβ profiles show great diversity, the mean Hβ profiles in 1972–1988 and in 1989–2001 are similar, although not identical. As can be seen from Table 4 and Figure 7, the broad Hβ profile in 1972–1988 was slightly narrower and slightly shifted to the blue compared to the average profile from 1989 to 2001.

We tested for correlations between the various Hβ profile parameters and with the continuum flux as well. A set of linear correlation coefficients based on the CCD spectra obtained in 1989–2001 is shown in Table 5. The values in parentheses are the probability that the correlation coefficient is less than zero (for negative coefficients) or that it is greater than zero (for positive coefficients).

[7] As an aid to understanding profile variations, we have made a movie that shows the variability of the Hβ profile in NGC 5548, based on many of the spectra described here. The movie can be accessed at http://www.astronomy.ohio-state.edu/~peterson/AGN/.

TABLE 5
CORRELATION COEFFICIENTS

Parameter	$F(\lambda5100)$	$F(\rm H\beta)$	Centroid	$\sigma_{\rm line}$	FWHM	EW	b/r
$F(\lambda5100)$	1	+0.914(1.000)	+0.036(0.560)	−0.257(0.856)	−0.127(0.686)	−0.724(1.000)	−0.127(0.692)
$F(\rm H\beta)$	+0.914(1.000)	1	−0.023(0.538)	−0.392(0.946)	−0.287(0.859)	−0.446(0.995)	−0.079(0.622)
Centroid	+0.036(0.560)	−0.023(0.538)	1	+0.072(0.615)	+0.107(0.659)	−0.055(0.619)	−0.924(1.000)
$\sigma_{\rm line}$	−0.257(0.856)	−0.392(0.946)	+0.072(0.615)	1	+0.898(1.000)	−0.048(0.601)	−0.209(0.790)
FWHM	−0.127(0.686)	−0.287(0.859)	+0.107(0.659)	+0.898(1.000)	1	−0.162(0.795)	−0.273(0.838)
EW	−0.724(1.000)	−0.446(0.995)	−0.055(0.619)	−0.048(0.601)	−0.162(0.795)	1	+0.113(0.724)
b/r	−0.127(0.692)	−0.079(0.622)	−0.924(1.000)	−0.209(0.790)	−0.273(0.838)	+0.113(0.724)	1

NOTE.—Given in parentheses are the probabilities for a test of the hypothesis that the correlation coefficient is less than zero (for negative coefficients) or that it is greater than zero (for positive coefficients), i.e., high or low tails of r-distribution with zero expectation value.

Since we consider all the profile parameters and the continuum light curve to be random processes and they consist of statistically dependent values, the number of degrees of freedom for the r-distribution was computed as described in the Appendix.

Table 5 shows that there are no significant correlations, except for the trivial correlations (e.g., a correlation between line and continuum fluxes or between profile centroid and blue-to-red ratio of the wing fluxes). The most significant correlation (95% confidence for the CCD spectra and 98% for the entire data set) is an inverse correlation between Hβ profile width $\sigma_{\rm line}$ and the Hβ total flux. This is consistent with the known correlation between lag and flux in NGC 5548 (Peterson et al. 2002) and the known inverse correlation between lag and line width expected for gravitationally dominated motion (Peterson & Wandel 1999). The same conclusions can be drawn from the spectra obtained in 1972–1988 if we exclude periods when the Hβ profile was evolving dramatically, and from the entire data set. Also, as noted previously, the Hβ equivalent width is inversely correlated with the optical continuum flux.

3. SUMMARY

We have analyzed 30 years of NGC 5548 Hβ emission-line and continuum variability based on archival pre-CCD spectra from 1972 to 1988 and CCD spectra obtained during the International AGN Watch campaign in 1989–2001. We reach the following conclusions:

1. The variability characteristics, such as mean fluxes, rms variability amplitude, autocorrelation functions, and cross-correlation results are found to be similar, within uncertainties, for the periods 1972–1988 and 1989–2001. The only significant difference is that the mean Hβ flux was higher for 1972–1988.

2. The mean Hβ profiles for 1972–1988 and 1989–2001 are very similar, although not identical, while the individual profiles show dramatic changes over several years or even less.

3. Examination of the Hβ-continuum relationship ($F_{\rm line} = aF_{\rm cont}^{b}$) suggests that this has changed somewhat between 1972–1988 and 1989–2001; the coefficient a has changed at the 2.6 σ confidence level, consistent with conclusion (1) above, although the difference in b does not seem to be statistically significant. For both time periods, the Hβ equivalent width is inversely correlated with the optical continuum flux, i.e., $b < 1$. We also find larger uncertainties in the coefficients of this relationship compared to the results of previous studies.

4. No significant correlations, except for trivial correlations, were found between various Hβ profile parameters (such as profile width, profile centroid, blue-to-red ratio of the wing fluxes) and continuum fluxes. The most significant correlation that was found (at 95% confidence for 1989–2001 and 98% confidence for the entire data set) is an inverse correlation between Hβ profile widths and the Hβ total fluxes, consistent with expectations for a virialized BLR.

5. In the Appendix, we have used the theory of random processes to compute uncertainties for the quantities derived from the time-series analysis. In particular, we have performed a Monte Carlo simulation of the observed light curves via random processes.

The present paper is dedicated to the memory of K. K. Chuvaev. He really pioneered spectroscopic monitoring of AGNs. The present study was possible only because of his observations of NGC 5548 during many years since 1972.

The research described in this publication was made possible in part by award UP1-2549-CR-03 of the US Civilian Research and Development Foundation for the Independent States of the Former Soviet Union (CRDF), by the Russian Foundation for Basic Research (RFBR) grant 06-02-16843, and by the National Science Foundation grant AST 06-04066.

APPENDIX A

DETERMINATION OF UNCERTAINTIES FOR RANDOM PROCESSES

Since a light curve is a set of statistically dependent values, i.e., a random process, simple formulae for the determination of uncertainties of random values are not applicable. In this section, we describe, without detailed mathematics, methods that have been used for the determination of uncertainties for the quantities obtained from these spectra, including mean fluxes, variability amplitudes, and correlation and regression coefficients. We also refer the reader to the relevant literature on time-series analysis, specifically Taylor (1997), Rencher (2002), Mason et al. (2003), and Chatfield (2003).

Let us assume that $x(t)$ is a stationary random process given as pairs (x_i, t_i), with $i = 1. \ . \ . \ n$. We will use the symbol E for the expectation value, the symbol D for variance, and $\sigma = \sqrt{D}$ for standard deviation.

A1. EXPECTATION VALUE

As an estimator for the expectation value E of the random process $x(t)$, we use the mean value

$$\langle x \rangle = \frac{1}{n} \sum_i x_i. \tag{A1}$$

Since the variance of a sum of statistically dependent values is

$$\sum_{i,j} \sigma(x_i)\sigma(x_j) r(x_i, x_j),$$

the variance of $\langle x \rangle$ must be equal to

$$D(\langle x \rangle) = \frac{D}{n^2} \sum_{i,j} r(x_i, x_j), \tag{A2}$$

where D is the variance of the random process $x(t)$, and $r(x_i, x_j)$ is a correlation coefficient between x_i and x_j, i.e., the autocorrelation function ACF(τ_{ij}), where $\tau_{ij} = t_i - t_j$. This is the same as finding uncertainties in the mean value with the "number" of data points (i.e., number of degrees of freedom) equal to

$$m_{\rm dof} = \frac{n^2}{\sum_{i,j} r(x_i, x_j)}. \tag{A3}$$

A2. VARIANCE

As an estimator for the variance D of the random process $x(t)$, we use the value

$$\langle x^2 \rangle - \langle x \rangle^2 = \frac{1}{n} \sum_i (x_i - \langle x \rangle)^2. \tag{A4}$$

Its variance is equal to

$$D(\langle x^2 \rangle - \langle x \rangle^2) = 2D^2 \left(\frac{1}{n^2} \sum_{i,j} r^2(x_i, x_j) + \frac{1}{m_{\rm dof}^2} - \frac{2}{n^3} \sum_{i,j,k} r(x_i, x_j) r(x_i, x_k) \right). \tag{A5}$$

The expectation value of the estimator $\langle x^2 \rangle - \langle x \rangle^2$ must be systematically displaced (biased) to D, since the exact value of $E(x)$ is unknown, and we use the mean value $\langle x \rangle$ instead. The unbiased value is equal to

$$(\langle x^2 \rangle - \langle x \rangle^2) \frac{m_{\rm dof}}{m_{\rm dof} - 1}. \tag{A6}$$

However, our computations show that it differs by only a few percent because our time series are very long, so that $m_{\rm dof} \gg 1$ (for the continuum light curve, we found $m_{\rm dof}$ to be 13.7 and 23.3 for the CCD and pre-CCD data, respectively, and for the Hβ light curve we found it to be 11.8 and 22.6). Finally, the variance of the rms variability amplitude is equal to

$$D(\sigma_x) = D\left(\sqrt{\langle x^2 \rangle - \langle x \rangle^2} \right) \approx \frac{D(\langle x^2 \rangle - \langle x \rangle^2)}{4(\langle x^2 \rangle - \langle x \rangle^2)}. \tag{A7}$$

A3. CORRELATION COEFFICIENT

Uncertainties in the correlation coefficient between the time series $x(t)$ and $y(t)$ have been computed via the r-distribution, but with the number of degrees of freedom modified to

$$r_{\rm dof} = \frac{n^2}{\sum_{i,j} r(x_i, x_j) r(y_i, y_j)}, \tag{A8}$$

where $r(x_i, x_j)$ and $r(y_i, y_j)$ are autocorrelation functions for $x(t)$ and $y(t)$, respectively. This is only applicable to the large data sampling ($r_{\rm dof} \gg 1$) and when $E(r) = 0$ or when the ACF for $x(t)$ is equal to the ACF for $y(t)$ and the CCF is a scaled version of ACF.

A4. REGRESSION COEFFICIENT

The regression coefficient b for the ordinary linear regression $y = a + bx$ can be computed as

$$b = \frac{c}{D_x} = r \frac{\sigma_y}{\sigma_x}, \tag{A9}$$

where c is a covariance function $\mathrm{Cov}(x, y) = \langle xy \rangle - \langle x \rangle \langle y \rangle$, $D_x = \langle x^2 \rangle - \langle x \rangle^2$, and r is a correlation coefficient between the $x(t)$ and $y(t)$ time series. Under large data sampling (large degree of freedom), the variance of b is equal to

$$D(b) = D\left(\frac{c}{D_x} \right) = \frac{D(c)}{D_x^2} + \frac{c^2 D(D_x)}{D_x^4} - \frac{2c\,\mathrm{Cov}(c, D_x)}{D_x^3}, \tag{A10}$$

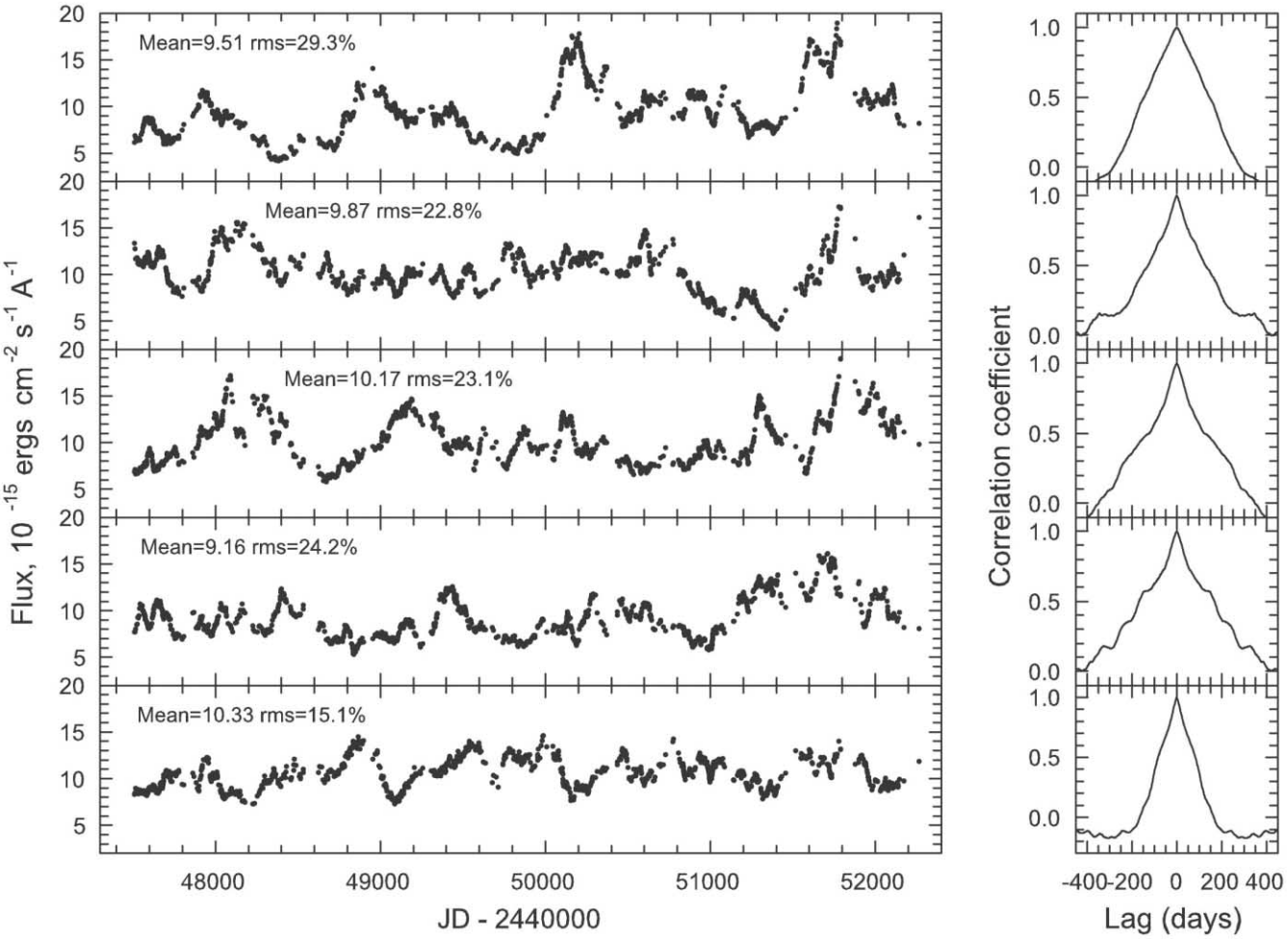


FIG. 8.—Simulations of the optical continuum light curve of NGC 5548 in 1989–2001 via random time series. The five left panels show the first five of 4000 realizations of the same random process with the autocorrelation function as computed from the observed continuum light curve. Mean flux and rms variability amplitude are shown for each of the five realizations, as well as the corresponding autocorrelation functions (*left panels*).

where $D(D_x)$ is computed from equation (A5), and where

$$D(c) = D(x)D(y)\left(\frac{1}{n^2}\left[\sum_{i,j} r(x_i,x_j)r(y_i,y_j) + \sum_{i,j} r(x_i,y_j)r(x_j,y_i)\right] + \frac{1}{n^4}\left\{\sum_{i,j} r(x_i,x_j)\sum_{i,j} r(y_i,y_j) + \left[\sum_{i,j} r(x_i,y_j)\right]^2\right\} - \frac{2}{n^3}\left[\sum_{i,j,k} r(x_i,x_j)r(y_i,y_k) + \sum_{i,j,k} r(x_i,y_j)r(x_k,y_i)\right]\right), \tag{A11}$$

$$\mathrm{Cov}(c,D_x) = 2D(y)^{1/2}D(x)^{3/2}\left\{\frac{1}{n^2}\sum_{i,j} r(x_i,x_j)r(x_j,y_i) + \frac{1}{n^4}\left[\sum_{i,j} r(x_i,x_j)\right]\left[\sum_{i,j} r(x_i,y_j)\right] - \frac{1}{n^3}\left[\sum_{i,j,k} r(x_i,x_j)r(x_k,y_i) + \sum_{i,j,k} r(x_i,x_j)r(x_i,y_k)\right]\right\}, \tag{A12}$$

where $r(x_i,x_j)$, $r(y_i,y_j)$, and $r(x_i,y_j)$ are auto- and cross-correlation functions for the $x(t)$ and $y(t)$ time series, and where $D(x)$ and $D(y)$ are variances of these two series. The unbiased estimators for $D(x)$ and $D(y)$ can be obtained via $\langle x^2\rangle - \langle x\rangle^2$ and $\langle y^2\rangle - \langle y\rangle^2$ according to equation (A6).

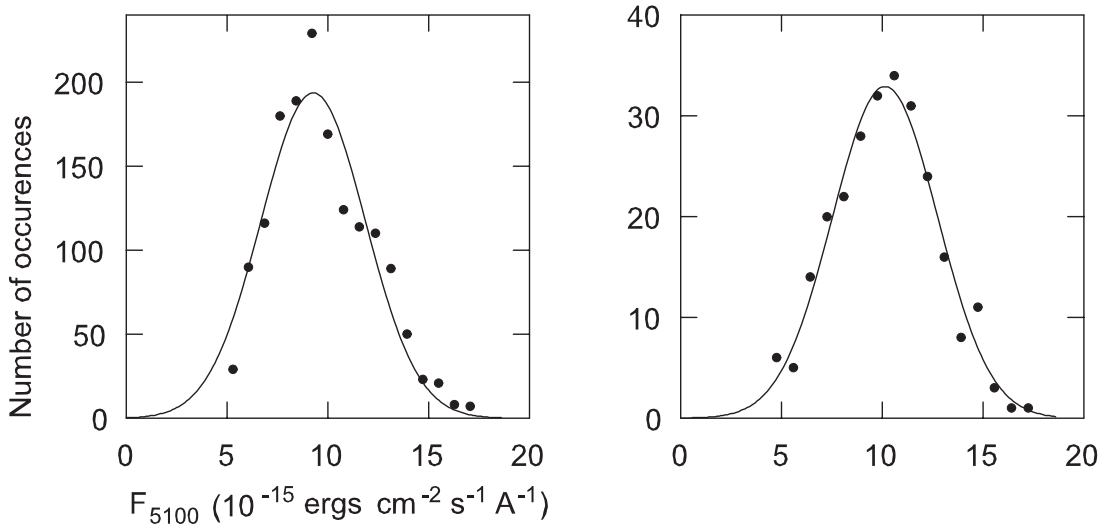


FIG. 9.—Histograms of the continuum light curve in 1972–1988 (*left panel*) and in 1989–2001 (*right panel*). Solid lines are Gaussian fits.

A5. REGRESSION CONSTANT

The regression constant a for ordinary linear regression $y = a + bx$ is $a = \langle y\rangle - b\langle x\rangle$. Its variance, under large data sampling, is therefore equal to

$$D(a) = D(\langle y\rangle - b\langle x\rangle) = D(\langle y\rangle) + \langle x\rangle^2 D(b) + b^2 D(\langle x\rangle) - 2b\mathrm{Cov}(\langle x\rangle, \langle y\rangle), \tag{A13}$$

where

$$\mathrm{Cov}(\langle x\rangle, \langle y\rangle) = \frac{1}{n^2} D(x)^{1/2} D(y)^{1/2} \sum_{i,j} r(x_i, y_j), \tag{A14}$$

and where $D(\langle x\rangle)$ and $D(\langle y\rangle)$ are computed from equation (A2), and equation (A10) is used to compute $D(b)$.

A6. WIDTH OF THE AUTOCORRELATION FUNCTION AND MONTE CARLO SIMULATION OF TIME SERIES

The uncertainties in the width of the autocorrelation function have been computed via a Monte Carlo simulation of random time series. We have generated random processes with the same autocorrelation function, mean value, and rms variability amplitude as the observed time series described in this paper. We have used the following algorithm to compute a realization of the random process with a given autocorrelation function ACF(τ): we have first generated an array of independent Gaussian deviates $\Delta x(t_i)$ for equidistantly spaced moments t_i with increment Δt. We have then convolved this array with some kernel of the convolution to be computed from ACF(τ). After the convolution operation, the values of $\Delta x(t_i)$ are statistically dependent, and they are represent the Gaussian random process with ACF(τ) equal to the convolution of this kernel with itself. We have then rebinned the simulated time series to the real times of observations. Since the increment Δt was adopted to be much less than one day, the effect of such rebinning is negligible. Finally, the same exponential transform has been applied to each realization for consistency with the observed mean flux and variability amplitude and to avoid negative values. In Figure 8, we show the first five of 4000 realizations of the random process that simulates the optical continuum light curve of NGC 5548 in 1989–2001. We found a good agreement between uncertainty estimates from the Monte Carlo simulations and those from the formulae given above. In Figure 9, we show a histogram of the observed continuum light curve. It can be seen that the observed process of the flux variations can indeed be roughly treated as a Gaussian process.

REFERENCES

Akritas, M. G., & Bershady, M. A. 1996, ApJ, 470, 706
Anderson, K. S. 1971, ApJ, 169, 449
Bentz, M. C., Peterson, B. M., Pogge, R. W., Vestergaard, M., & Onken, C. A. 2006, ApJ, 644, 133
Blandford, R. D., & McKee, C. F. 1982, ApJ, 255, 419
Byard, P. L., Foltz, C. B., Jenkner, H., & Peterson, B. M. 1981, PASP, 93, 147
Cackett, E. M., & Horne, K. 2006, MNRAS, 365, 1180
Chakrabarti, S. K., & Wiita, P. J. 1994, ApJ, 434, 518
Chatfield, C. 2003, The Analysis of Time Series: An Introduction (6th ed.; London: Chapman & Hall/CRC)
Chuvaev, K. K. 1987, in IAU Symp. 121, Observational Evidence of Activity in Galaxies, ed. E. E. Khachikian, K. J. Fricke, & J. Melnick (Dordrecht: Kluwer), 203
Clavel, J., et al. 1991, ApJ, 366, 64
Gaskell, C. M. 1983, in Quasars and Gravitational Lenses, ed. J.-P. Swings (Cointe-Ougree: Univ. Liége), 471
———. 1996, ApJ, 464, L107
Gaskell, C. M., & Peterson, B. M. 1987, ApJS, 65, 1
Gaskell, C. M., & Sparke, L. S. 1986, ApJ, 305, 175
Gilbert, A. M., Eracleous, M., Filippenko, A. V., & Halpern, J. P. 1999, in ASP Conf. Ser. 175, Structure and Kinematics of Quasar Broad-Line Regions, ed. C. M. Gaskell et al. (San Francisco: ASP), 189
Gilbert, K. M., & Peterson, B. M. 2003, ApJ, 587, 123
Goad, M., & Wanders, I. 1996, ApJ, 469, 113
Goad, M. R., Korista, K. T., & Knigge, C. 2004, MNRAS, 352, 277

Kinney, A. L., Rivolo, A. R., & Koratkar, A. P. 1990, ApJ, 357, 338
Korista, K. T., & Goad, M. R. 2004, ApJ, 606, 749
Korista, K. T., et al. 1995, ApJS, 97, 285
Markowitz, A., & Edelson, R. 2004, ApJ, 617, 939
Marshall, H. L., et al. 1997, ApJ, 479, 222
Mason, R. L., Gunst, R. F., & Hess, J. L. 2003, Statistical Design and Analysis of Experiments (2nd ed.; New York: Wiley Interscience)
Peterson, B. M. 1987, ApJ, 312, 79
———. 1993, PASP, 105, 247
Peterson, B. M., Korista, K. T., & Cota, S. A. 1987, ApJ, 312, L1
Peterson, B. M., Korista, K. T., Wagner, R. M., & Reichert, G. A. 1990, ApJ, 352, 68
Peterson, B. M., & Wandel, A. 1999, ApJ, 521, L95
Peterson, B. M., Wanders, I., Horne, K., Collier, S., Alexander, T., Kaspi, S., & Maoz, D. 1998, PASP, 110, 660
Peterson, B. M., et al. 1991, ApJ, 368, 119
———. 1994, ApJ, 425, 622
———. 2002, ApJ, 581, 197
Peterson, B. M., et al. 2004, ApJ, 613, 682
Pogge, R. W., & Peterson, B. M. 1992, AJ, 103, 1084
Rencher, A. C. 2002, Methods of Multivariate Analysis (2nd ed.; New York: Wiley Interscience)
Romanishin, W., et al. 1995, ApJ, 455, 516
Sergeev, S. G., Pronik, V. I., & Sergeeva, E. A. 2000, A&A, 356, 41
———. 2001, ApJ, 554, 245
Stirpe, G. M., de Bruyn, A. G., & van Groningen, E. 1988, A&A, 200, 9
Taylor, J. 1997, An Introduction to Error Analysis (2nd ed.; Sausalito: Univ. Science Books)
van Groningen, E., & Wanders, I. 1992, PASP, 104, 700
Veilleux, S., & Zheng, W. 1991, ApJ, 377, 89
Wamsteker, W., et al. 1990, ApJ, 354, 446
Wanders, I., & Peterson, B. M. 1996, ApJ, 466, 174
Wanders, I., et al. 1995, ApJ, 453, L87
White, R. J., & Peterson, B. M. 1994, PASP, 106, 879
Zheng, W., Veilleux, S., & Grandi, S. A. 1991, ApJ, 381, 418